THE JOURNAL OF BIOLOGICAL CHEMISTRY VOL. 286, NO. 48, pp. 41217–41229, December 2, 2011

Sequence TTKF ↓ QE Defines the Site of Proteolytic Cleavage in Mhp683 Protein, a Novel Glycosaminoglycan and Cilium Adhesin of *Mycoplasma hyopneumoniae*[*] [S]

Received for publication, January 28, 2011, and in revised form, July 18, 2011 Published, JBC Papers in Press, October 3, 2011, DOI 10.1074/jbc.M111.226084

Daniel R. Bogema[‡§1], Nichollas E. Scott[¶], Matthew P. Padula[‖], Jessica L. Tacchi[‖], Benjamin B. A. Raymond[‖], Cheryl Jenkins[‡], Stuart J. Cordwell[¶], F. Chris Minion[**], Mark J. Walker[§‡‡], and Steven P. Djordjevic[‡‖2]

From the [‡]NSW Department of Primary Industries, Elizabeth Macarthur Agricultural Institute, Camden 2567, New South Wales, Australia, the [§]School of Biological Sciences, University of Wollongong, Wollongong 2522, New South Wales, Australia, the [¶]School of Molecular and Microbial Biosciences, University of Sydney, Sydney 2006, New South Wales, Australia, [‖]The ithree Institute, University of Technology, Sydney 2007, New South Wales, Australia, [**]Veterinary Microbiology and Preventive Medicine, Iowa State University, Ames, Iowa 50011, and the [‡‡]School of Chemistry and Molecular Biosciences and the Australian Infectious Diseases Research Centre, University of Queensland, Brisbane 4072, Queensland, Australia

Mycoplasma hyopneumoniae* colonizes the ciliated respiratory epithelium of swine, disrupting mucociliary function and inducing chronic inflammation. P97 and P102 family members are major surface proteins of *M. hyopneumoniae* and play key roles in colonizing cilia via interactions with glycosaminoglycans and mucin. The *p102* paralog, *mhp683*, and homologs in strains from different geographic origins encode a 135-kDa preprotein (P135) that is cleaved into three fragments identified here as $P45_{683}$, $P48_{683}$, and $P50_{683}$. A peptide sequence (TTKF ↓ QE) was identified surrounding both cleavage sites in Mhp683. N-terminal sequences of $P48_{683}$ and $P50_{683}$, determined by Edman degradation and mass spectrometry, confirmed cleavage after the phenylalanine residue. A similar proteolytic cleavage site was identified by mass spectrometry in another paralog of the P97/P102 family. Trypsin digestion and surface biotinylation studies showed that $P45_{683}$, $P48_{683}$, and $P50_{683}$ reside on the *M. hyopneumoniae* cell surface. Binding assays of recombinant proteins $F1_{683}$–$F5_{683}$, spanning Mhp683, showed saturable and dose-dependent binding to biotinylated heparin that was inhibited by unlabeled heparin, fucoidan, and mucin. $F1_{683}$–$F5_{683}$ also bound porcine epithelial cilia, and antisera to $F2_{683}$ and $F5_{683}$ significantly inhibited cilium binding by *M. hyopneumoniae* cells. These data suggest that $P45_{683}$, $P48_{683}$, and $P50_{683}$ each display cilium- and proteoglycan-binding sites. Mhp683 is the first characterized glycosaminoglycan-binding member of the P102 family.

Mycoplasma hyopneumoniae is a global pathogen that inflicts severe economic losses on swine production (1, 2). Current treatment relies on the application of bacterin vaccine formulations that fail to block colonization of respiratory tract cilia and strategic antibiotic therapy. The development of more effective vaccines requires a detailed understanding of the molecular interactions that govern adherence and colonization of the porcine respiratory tract and involve adjuvant formulations that stimulate mucosal immunity (3–8).

M. hyopneumoniae is strictly a pathogen of swine, and alternate hosts or intermediary vectors have not been identified. Electron microscopic studies of infected lung tissues show that *M. hyopneumoniae* interacts almost exclusively with cilia on the epithelial surfaces that line the trachea, bronchi, and bronchioles in the porcine upper respiratory tract. Specifically, this microorganism is found attached along the entire length of the cilia but rarely to the epithelial cell body (9–11). To survive and proliferate as an infectious agent, *M. hyopneumoniae* must enter the respiratory tract of its host, traverse mucous layers, resist the mucociliary escalator, adhere and colonize epithelial cilia, secure essential nutrients for growth and replication, evade immune responses, and repeat the cycle of infection by transmission to new hosts via airborne mucosal droplets. Colonization of the upper respiratory tract by *M. hyopneumoniae* results in the destruction of the mucociliary escalator via ciliostasis, loss of cilia, and eventual epithelial cell death. The underlying mechanisms, however, are poorly understood (9). Once colonized, swine become chronically infected, but the strategies required to maintain a chronic infection state are ill defined. The mechanism utilized by *M. hyopneumoniae* to colonize respiratory cilia is likely to require multiple adhesins and strategies for avoiding immune detection.

Unlike the human respiratory pathogen *Mycoplasma pneumoniae*, *M. hyopneumoniae* does not display a complex terminal organelle and is not known to be motile, yet it is able to circumvent the protective effects of the mucociliary escalator in the porcine respiratory tract. P97, P102, and paralogs of these two molecules play important roles in interactions between *M. hyopneumoniae* and receptors in the porcine respiratory tract. mRNA transcripts representative of all members of the P97 and P102 paralog families (except Mhp280) are known to be expressed *in vivo* (12). Previous proteomic studies have determined that cleavage products of Mhp182 (P102), Mhp183 (P97), Mhp493 (P159), and Mhp494 (P216) are prominently featured on the surface of *M. hyopneumoniae* (13–15), whereas

* This work was supported by ARC-Linkage Grant LP776711 and a grant from the McGarvie Smith Trust (to S. P. D.).
[S] The on-line version of this article (available at http://www.jbc.org) contains supplemental Table 1, Figs. 1–4, and Data 1–5.
[1] Recipient of an Australian postgraduate award (Industry).
[2] To whom correspondence should be addressed: P. O. Box 123, Broadway, New South Wales 2007, Australia. Tel.: 61-2-9514-4127; Fax: 61-2-9514-4143; E-mail: steven.djordjevic@uts.edu.au.

others (Mhp271, Mhp107, and Mhp108) are expressed at lower levels (16–18). Tandem pentapeptide repeats (AAKP(V/E)) in the R1 domain of P97 (19, 20) play an important role in cilium binding. Non-R1-containing members of the P97 family also bind porcine cilia (15, 18) and epithelial cell surfaces (13, 18). The P97 paralog Mhp107 also binds plasminogen, fibronectin, and the glycosaminoglycan heparin (18). Mhp108, a member of the P102 family, binds cilia, fibronectin, and plasminogen (17), and domains within Mhp183, Mhp494, Mhp493, and Mhp271 bind heparin. Heparan sulfate includes regions within proteoglycan side chains that have been identified at the surface of porcine respiratory cilia (21). Heparin, a structural analog of the highly sulfated regions of heparan sulfate proteoglycans, effectively blocks the binding of *M. hyopneumoniae* to porcine cilia and to porcine kidney epithelium-like cells used previously as a cilial binding model (13, 22, 23). These observations underscore the diverse nature of cilium- and extracellular matrix binding domains presented by the P97 and P102 family of adhesins.

A hallmark feature of these two adhesin families is their tendency to be targets for precise proteolytic cleavage events that generate a complex array of binding domains. In the absence of recognized membrane anchorage motifs, the cleavage fragments adhere to the external membrane surface of *M. hyopneumoniae* and define discrete domains that bind cilia and a variety of host molecules, including fibronectin, various glycosaminoglycans, and plasminogen. Proteolytic processing is observed in all currently characterized members of the P97/P102 family.

Bioinformatic analysis of the genome sequence of *M. hyopneumoniae* has identified six P102 paralogs, defined as 30% identity over 70% of the sequence (24). Many of these P102 paralogs comprise two-gene structures with a P97 paralog (24, 25). Compared with P97 and its paralogs, the functions of P102 and related molecules are poorly understood. Cell lysates probed with antisera raised against recombinant P102 identified three proteins with masses of 102 kDa (pre-protein), 72 kDa (P72), and 42 kDa (P42) (12, 14). Immunogold electron microscopy studies of *M. hyopneumoniae* (14) harvested from broth culture and associated with cilia in infected lung tissue identified P102 and its cleavage fragments on the external surface of *Mycoplasma* cells and on the surface of porcine cilia (12). These data indicate that P102 is subject to proteolytic cleavage and plays a role in the colonization of the porcine respiratory tract. Many bacterial adhesins display complex cleavage or degradation patterns, which have not been extensively characterized, including several adhesins expressed by the phylogenetically related streptococci (26–29). Recently, we showed that the P102 paralog, Mhp108, is a proteolytically processed, multifunctional adhesin that binds fibronectin and plasminogen and adheres to porcine respiratory cilia (17). In this study, we have extensively characterized Mhp683, a member of the P102 family that forms part of a two-gene operon with P146, as an adhesin-like P97 paralog (24, 25).

EXPERIMENTAL PROCEDURES

M. hyopneumoniae Strains and Culture—The source and conditions used to culture *M. hyopneumoniae* strains J, 232, and field isolates 00MP1301, 2-2241, and 95MP1509 have been described previously (16, 30). *M. hyopneumoniae* isolate C1735-2 was isolated from a piggery in Queensland, Australia, and was provided by J. Forbes-Faulkner (Oonoonba Veterinary Laboratory, Queensland, Australia). *M. hyopneumoniae* cells were centrifuged at 10,000 × *g* and washed three times in PBS. Final pellets were stored at −20 °C until required.

Proteomics—Separation of *Mycoplasma* proteins into hydrophobic and hydrophilic fractions using Triton X-114 was performed prior to electrophoresis as described previously (31). Hydrophilic proteins of the aqueous phase were precipitated with cold acetone and resuspended in SSS buffer (8 M urea, 100 mM DTT, 4% (w/v) CHAPS, 0.8% (w/v) 3–10 carrier ampholytes, 40 mM Tris-HCl) for separation by electrophoresis.

Materials and methods used for one- and two-dimensional gel electrophoresis, immunoblotting, trypsin digestion, reduction and alkylation, Zip-Tip® clean-up, and peptide mass-mapping using matrix-assisted laser desorption-ionization time-of-flight mass spectrometry (MALDI-TOF MS) have been described previously (14, 16, 32) with the following adjustments. First dimension immobilized pH-gradient strips (ReadyStrip™ IPG Strips, 170 mm in length, nonlinear pH 3–10; Bio-Rad) were used. Strips were rehydrated overnight with 500 μg of Triton X-114 aqueous fraction protein extract in 360 μl of SSS buffer overlaid with paraffin oil. *M. hyopneumoniae* proteins were reduced prior to one-dimensional gel electrophoresis. Gel slices prepared from one-dimensional SDS-PAGE for tandem mass spectrometry analysis were processed as described previously (16). Protein spots excised from two-dimensional gels were processed as described previously (33, 34). Briefly, spots were excised using a sterile scalpel blade and washed in a destain solution (60:40 solution of 40 mM ammonium bicarbonate (pH 7.8), 100% acetonitrile) for 1 h at room temperature. The solution was removed from the wells, and the gel pieces were vacuum-dried for 1 h. The gel spots were rehydrated in 8 μl of trypsin solution (2 ng μl^{-1} (sequencing-grade modified trypsin (Promega, Madison WI) in 40 mM ammonium bicarbonate)) at 4 °C for 1 h. Excess trypsin was removed, and the gel pieces were resuspended in 25 μl of 40 mM ammonium bicarbonate and incubated overnight at 37 °C. Peptides were concentrated and desalted using C_{18} Perfect Pure™ tips (Eppendorf, Hamburg, Germany) and eluted in matrix (α-cyano-4-hydroxycinnamic acid (Sigma), 8 mg ml^{-1} in 70% (v/v) acetonitrile, 1% (v/v) formic acid) directly onto a target plate. Peptide mass maps were generated by matrix-assisted laser desorption/ionization time-of-flight mass spectrometry (MALDI-TOF MS) using a Voyager DE-STR (Applied Biosystems, Framingham MA). Mass calibration was performed using trypsin autolysis peaks, *m/z* 2211.11 and *m/z* 842.51 as internal standards. Data from peptide mass maps were used to perform searches of the NCBI, Swiss-Prot, and TrEMBL databases, via the program MASCOT. Identification parameters included peptide mass accuracy within 50 ppm, one possible missed tryptic cleavage per peptide, and with the methionine sulfoxide and cysteine acrylamide modifications checked. Identifications were based on MASCOT score and E-values, the observed pI and molecular mass (kDa) of the protein, the number of matching peptide masses, and the total percentage of the amino acid sequence that those peptides covered. Liquid chromatography coupled to tandem mass spectrometry (LC-MS/MS) analysis of

one- and two-dimensional electrophoresis gel excisions were performed as described previously (35) except that MASCOT searches were performed with additional variable modifications of deamidation (Asn, Gln) and Gln→pyro-Glu (N-terminal Gln and Glu).

Surface Localization—Graded trypsin digestion of intact *M. hyopneumoniae* for Western blotting was performed as described previously (14). Trypsin concentrations of 0, 0.1, 0.5, 1, 3, 5, 10, 50, and 300 μg ml^{-1} were used in this study. Trypsin digestion of intact *M. hyopneumoniae* for mass spectrometry was performed as described previously (16).

For surface biotinylation experiments, freshly harvested *M. hyopneumoniae* cells were washed extensively (>3 times) in PBS (4000 × *g*, 30 min, 4 °C) and pelleted by centrifugation (9000 × *g*, 10 min, 4 °C). Cells were resuspended in PBS (pH 7.8) and biotinylated with sulfo-NHS-LC biotin (Thermo Scientific) for 30 s on ice. The reaction was then quenched with the addition of a final concentration of 50 mM Tris-HCl (pH 7.4) and incubated for 15 min. Cells were washed in three changes of PBS and pelleted by centrifugation. A 0.1 g pellet of *M. hyopneumoniae* cells was resuspended in solubilization buffer (7 M urea, 2 M thiourea, 40 mM Tris (pH 8.8), 1% (w/v) C7bZ0) and disrupted with four rounds of sonication at 50% power for 30 s bursts on ice. Proteins were reduced and alkylated with 20 mM acrylamide monomers, 5 mM tributylphosphine for 90 min. Insoluble material was pelleted by centrifugation. Soluble proteins were precipitated in 5 volumes of ice-cold acetone for 30 min, and the pellet was air-dried and then resuspended in 7 M urea, 2 M thiourea, 1% (w/v) C7bZ0. Biotinylated proteins were purified by avidin column affinity chromatography performed as described previously (36). Biotinylated proteins were separated by two-dimensional gel electrophoresis and identified by Western blotting. Spots corresponding to biotinylated proteins were cut from simultaneously run two-dimensional gels and examined using LC-MS/MS.

Bioinformatic Analysis—Bioinformatic analysis of Mhp683 was performed with the use of several on-line resources. Sequence similarity was compared by BLASTP analysis of Mhp683 at the National Center for Biotechnology Information (37, 38) (www.ncbi.nlm.nih.gov). Physical data such as theoretical pI, molecular weight, and extinction coefficients were collected using the ProtParam tool at ExPASy (39). Identification of coiled-coil domains was performed using the COILS2 algorithm at the Swiss node of EMBnet (40) as well as Multicoil and Paircoil2 at the Massachusetts Institute of Technology (41, 42). Theoretical transmembrane domain and signal peptide scores were identified using the TMHMM and SignalP web services, respectively, at the Center for Biological Sequence Analysis, Technical University of Denmark (43–45). Prediction of disordered regions was performed using the Predictor of Naturally Disordered Regions (PONDR), VSL1 algorithm (46, 47).

Expression of Recombinant Proteins and Creation of Polyclonal Antisera—As *Mycoplasma* species use the UGA codon to translate tryptophan instead of signaling the end of translation, the expression of *Mycoplasma* proteins in *Escherichia coli* results in truncations. Cloning of *mhp*683 was performed in five fragments of varying length with minimal overlap (Fig. 3*A*) and was based on the *M. hyopneumoniae* strain 232 homolog (24); fragment size was largely determined by the presence of eight in-frame TGA codons. Fragments were labeled $F1_{683}$ through $F5_{683}$ and ranged from amino acids 42–308, 306–597, 595–803, 801–1017, and 1018–1194, respectively. All in-frame TGA codons were mutated to TGG by using mutated primers or site-directed mutagenesis (supplemental Table 1). Fragments were amplified by PCR from chromosomal *M. hyopneumoniae* strain 232 DNA using Pwo polymerase (Roche Applied Science) and cloned into the pET161/GW/D-TOPO vector (Invitrogen). The reaction mixture was then transformed into TOP10 chemically competent *E. coli* and incubated overnight at 37 °C in LB agar containing 100 μg ml^{-1} ampicillin (Sigma). Positive colonies were cultured further in LB media containing 100 μg ml^{-1} ampicillin (Sigma) and plasmids extracted with the QIAprep Spin Miniprep Kit (Qiagen, Netherlands). Purified plasmids were screened for correct orientation by PCR and sequenced to check for mutations.

Protein expression was achieved by use of the *E. coli* BL21Star™ strain (Invitrogen). Plasmids were transformed and inoculated into LB media containing 100 μg ml^{-1} ampicillin and cultured at 37 °C overnight. A subculture was performed the following day and allowed to grow to mid-log phase (A_{600} = 0.5–0.8) before induction of expression with 1 mM isopropyl β-D-1-thiogalactopyranoside and incubation for 3–4 h. $F1_{683}$–$F5_{683}$ were purified by nickel affinity chromatography and dialyzed in PBS containing 0.1% SDS (Fig. 3*B*), and their concentrations were estimated as described previously (48).

Polyclonal antisera to recombinant proteins $F1_{683}$–$F5_{683}$ were prepared by immunization of New Zealand White Rabbits as described previously (49). All antisera were tested for activity by immunoblots with recombinant protein (Fig. 3*C*).

Heparin Binding Assays—Heparin binding, inhibition, and competitive immunoassays were performed in 96-well, flat-bottomed microtiter plates (Linbro/Titertek; ICN Biomedicals Inc., Aurora, OH) with binding steps all performed in a volume of 100 μl. For heparin binding assays, proteins ($F1_{683}$–$F5_{683}$) were diluted to 10 μg ml^{-1} in carbonate coating buffer (18 mM $NaHCO_3$, 27 mM Na_2CO_3 (pH 9.5)) and bound to plates by shaking on a Titramax 1000 microtiter plate shaker (Heidolph, Schwabach, Germany) at room temperature for 2 h; unbound and excess protein were removed by immersing wells five times in wash buffer (0.05% Tween 20 in PBS). Pre-diluted biotinylated heparin (Calbiochem) was added to wells in serial 2-fold dilutions starting from 100 μg ml^{-1}, and plates were incubated at room temperature for 1 h with shaking. The plates were again immersed five times in wash buffer followed by addition of streptavidin/peroxidase (Roche Applied Science) at a dilution of 1:3000 in PBS and incubated with shaking for 1 h. After a final wash step, the plates were developed with 1 mM 2,2′-azinobis(3-ethylbenzothiazoline-6-sulfonic acid) (Sigma) in citrate buffer (100 mM citric acid, 200 mM sodium hydrogen phosphate di-basic (pH 4.2)) treated with hydrogen peroxide. Plates were developed with shaking, and the absorbance at 414 nm was measured at 7-, 15-, 25-, and 45-min intervals.

Heparin binding specificity and competitive binding assays were performed as described previously (48). All heparin binding assays were performed in triplicate with previously stated controls (48) and graphed by GraphPad Prism Version 4.02 for

MNQFDEKEKQHNKAKAILSTGFSVTSIATTVVAVPIGLTIFEKSFSSQVSGGVDK
NKVVDLK**SDSDLIFSEEDFIR**AVENLKLFDKYRHLTARMALGLAR**EAANAFNFLD**
TYDYTPITKHSFK**ISLDISDAFAANK**EVKAVVVSAYSQKYQVTYSRLTSLKGWKE
EDDFGDDIIDYQINQELSGLSLSSLAPESAHLLASEMAFR**LDNDFQVAYK**KTGSR
AEAFRQALIKNYLGYNLVNRQGLPTMLQKGYVLAPKTIENKNASEEKLVNINEND
RARVNKLQKVENLAFKNLSDPNGTLSITFELWDPNGKLVSEYDFKIKGIKKLDFD
LKKQEEKVLQKVTEFVEIKPYVQLGLIRDNLSLSEIIYKNDNNPEYLRKILDKLK
EHNNNKKVDNNTSTTKFQEEDLKNEPNSNGSEQDSFEKAK**ENFLSFFDLR**SRLIP
IPDLPLYYLKVNSINFDRNIEENEKEK**LLENEQVVLK**VDFSLKKVVSDIR**APYLV**
SSQVRSNYPPVLKASLAKIGKGSNSK**VVLLDLGNLSSR**FKVQLDYSAKQREIINT
LLKENPEREKELQAKIESKTFSPIDLNNDDLLAIEFQYEDNPEGDWITLGRMEKL
VKEVIQYKKEGKTFLDDEVAKTLYYLDFHHLPQSKKDLEEYKEKHKNKFINEIKP
ATATSQAKPDQAKNEKEVKPESAQAESSSSNSNDSNSKTTSSSSMAGTTQNKSTE
TPNSSSNSTPTSSATTSTTSSTQAAATSASSAKVKTTKFQEQEKQQVKEQKQKQE
KTKETNQLLDTKTNKENLGLGLILWDFLVNSKYK**TLPGTTWDFLVEPDSFNDR**LK
ITAILKENTSQAKSNPDSKNLTSLTRNLIIKGVMANK**YIDYLVQEDPVLLVDYTR**
RNQIKTER**EGQLIWSQLASPQMASPEPEK**TKLEITEEGLRVKKGGTKIKEGIKNG
SSRGNTNTNSKPNKKLVLLKGAIKNPGTKKEWILVGSGIKDNNNGGSNNNSNTQI
WITRLGTSVGSLK**TEGETVLGISNNNSQGEVLWTTIK**SK**LENENPSDNNQIQYSP**
STHSLTTNSRSNTQQSGRNQIKITNTQR**KTTTSPSQNLSQNPDPNQIDVRLGLLV**
QDKKLHLWWIANDSSDEPEHITIDFAEGTK**FNYDDLNYVGGLLK**NTTNNNNTQAQ
DDEGDGYLALK**GLGIYEFPDDESIDQAATVEK**AERLYKHFMGLFRE

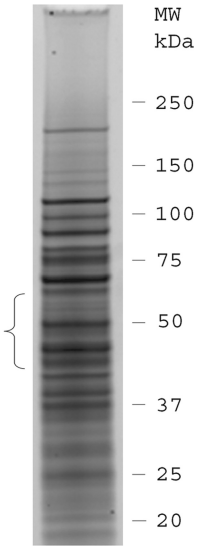

FIGURE 1. **Expected molecular weight of MHJ_0622 (the Mhp683 homolog in strain J) is not reflected in peptide analysis.** Gel image showing cell lysate (100 μg) of *M. hyopneumoniae* strain J separated by SDS-PAGE and stained with Flamingo™ fluorescent stain. The gel lane was sectioned into pieces representing 14 molecular weight ranges, and each piece was digested with trypsin. Peptides from the gel piece representing a 40–55 kDa mass range were identified by LC-MS/MS (*underlined* in *bold*) and matched to regions of MHJ_0662. No peptides matching to MHJ_0662 were identified in proteins resolving at ~135 kDa, the predicted mass of the MHJ_0662.

Microsoft Windows (Graphpad Software, CA) by nonlinear regression.

Heparin binding dot-blots were performed using the Bio-Dot® microfiltration apparatus (Bio-Rad). Hybond Super-C nitrocellulose membrane (Amersham Biosciences) was equilibrated in PBS and fastened into the apparatus. Proteins were added to the wells in serial 2-fold dilutions starting from 1 μg. Proteins were allowed to bind for 1 h or until the solution had drained through the membrane. Unbound protein was removed by washing with 100 μl of PBS. The membrane was removed from the manifold and blocked with 5% skim milk blocking buffer (5% skim milk, 10 mM Tris, 150 mM sodium chloride (pH 7.4)) for 1 h with shaking. The membrane was then immersed in 0.1% skim milk wash buffer (0.1% skim milk, 10 mM Tris, 150 mM sodium chloride (pH 7.4)) containing 30 μg ml^{-1} biotinylated heparin with shaking for 90 min. After three vigorous washes, the membrane was immersed in a solution of 1 part streptavidin and 3000 parts 0.1% skim milk wash buffer for 1 h with shaking. Following another wash step (as before), the membrane was equilibrated in 100 mM Tris (pH 7.6) solution and developed with 0.05% diaminobenzidine dissolved in 100 mM Tris (pH 7.6) and treated with hydrogen peroxide.

Cilium Binding and Inhibition Assays—The binding of Mhp683 to porcine cilia was examined as described previously using a microtiter plate adherence assay developed for the identification of the cilium-binding protein P97 (15). Inhibition of *M. hyopneumoniae* adherence to porcine cilia by Mhp683 antisera was examined using the microtiter plate adherence assay with the following adjustments. Plates were coated in cilia as described previously (15) and blocked for 1 h with 1% gelatin (Sigma) in PBS. Freshly cultured *M. hyopneumoniae* cells were washed twice, resuspended in PBS at 1:200 of the original culture volume, and then incubated with a 1:50 dilution of antisera for 1 h. Following antisera treatment, cells were added directly to cilia-coated wells, incubated for 1.5 h, and washed three times with PBS. Mycoplasmas were detected by subsequent addition of mouse monoclonal antibody F1B6 diluted to 1:250 and alkaline phosphatase-conjugated anti-mouse antibodies (1:1000) absorbed against rabbit antibodies.

RESULTS

Mhp683 Is Proteolytically Cleaved—In strain 232, *mhp683* encodes a P102 paralog with a theoretical molecular mass of 135 kDa and a theoretical pI of 7.2. Homologs of *mhp683* exist within other *M. hyopneumoniae* genome sequences and are referred to as *mhj_0662* in strain J and *mhp7448_0662* in strain 7448. These homologs encode proteins that share 94% amino acid sequence identity that are referred to collectively here as Mhp683. The TMHMM algorithm identified a transmembrane domain ($p = 0.973$) from residues 17 to 39 in both *M. hyopneumoniae* strains J and 232, indicating the presence of a putative signal peptide; however, analysis of Mhp683 with SignalP resulted in a low signal peptide probability ($p = 0.409$, signal peptide cutoff of $p > 0.5$).

To determine whether Mhp683 is expressed during growth in broth culture, we adopted an approach combining one-dimensional SDS-PAGE and LC-MS/MS. Global analysis of strain J proteins that migrated in an SDS-polyacrylamide gel with masses from ~45 to 55 kDa identified a panel of tryptic peptides that mapped across the Mhp683 sequence (Fig. 1). These data suggested that Mhp683 was a target of post-translational cleavage events that cleave the molecule in three fragments each with a mass of 45–55 kDa. MALDI-TOF-MS and LC-MS/MS of protein spots separated by two-dimensional gel electrophoresis identified several distinct groups of protein spots that mapped to three nonoverlapping regions of Mhp683. An N-terminal cleavage product ($P45_{683}$; Fig. 2*A*) was matched from a linear pattern of four spots at ~45 kDa with pI values ranging from 8 to 10. Proteins that mapped to the central region of Mhp683 ($P48_{683}$; Fig. 2*A*) were identified in two spots with pI

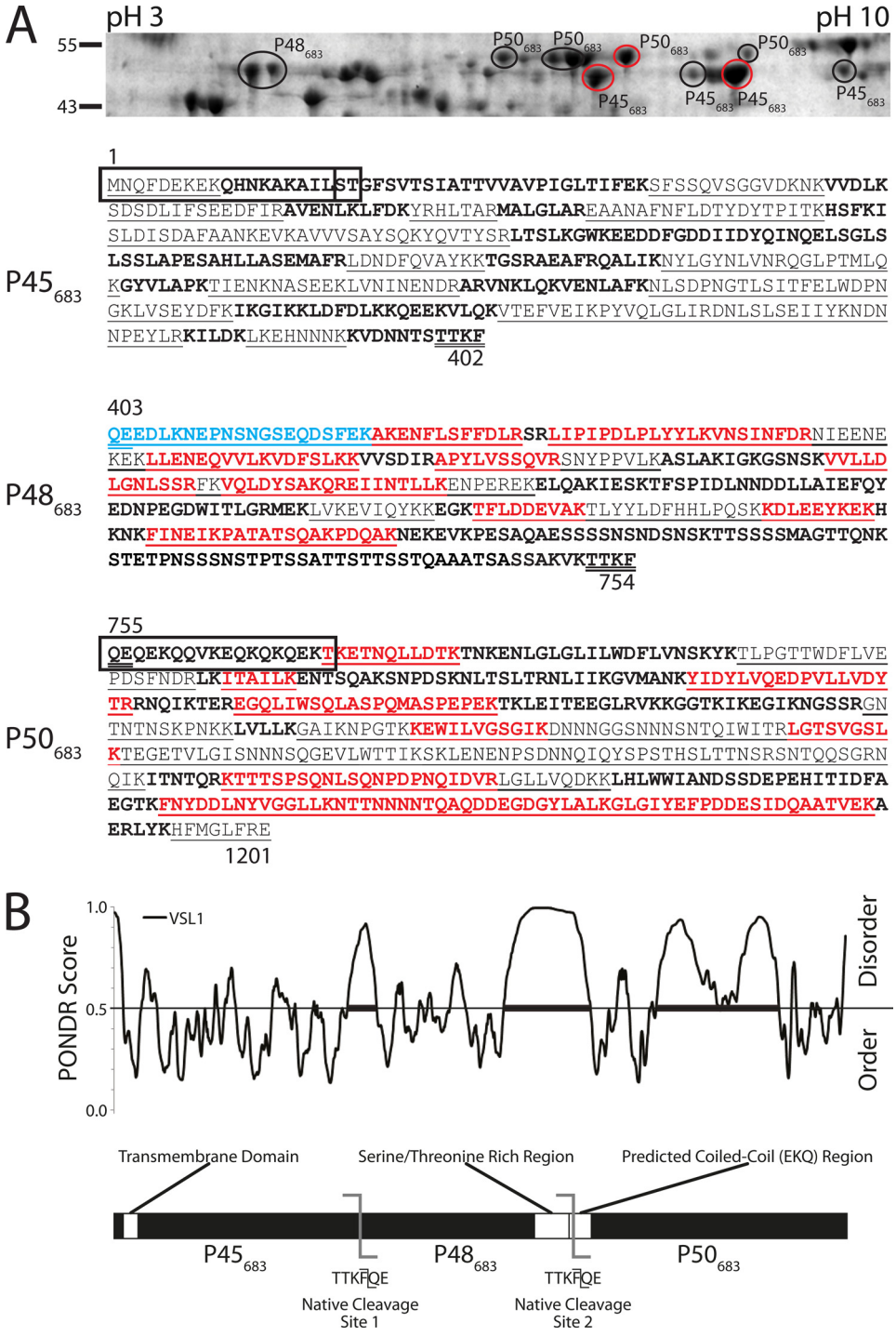

FIGURE 2. *A,* two-dimensional gel electrophoresis, mass spectrometry, and N-terminal sequencing confirms MHJ_0662 is cleaved into three fragments of approximately equal size. Coomassie-stained two-dimensional gel of a cell lysate of *M. hyopneumoniae* strain J depicts proteins with masses between 43 and 55 kDa. Protein spots were excised from the gel, digested with trypsin, and identified by peptide-mass fingerprinting with MALDI-TOF-MS, where trypsin-digested peptides are identified by matching peaks to the calculated masses of predicted fragments. Protein spots were also identified by LC-MS/MS, where trypsin-digested peptides are directly sequenced using tandem mass spectrometry. Peptides identified by MALDI-TOF-MS are *underlined*; peptides identified by LC-MS/MS are shown in *bold, red,* and *underlined*; sequences not identified by either technique are in *bold*. Peptides from MHJ_0662 (Mhp683 homolog in strain J) were identified in spots localizing to three distinct regions (*circled*) of the gel with masses of 45–55 kDa and varying isoelectric points. Cleavage fragments spanning the amino, central, and carboxyl portions of MHJ_0662 are labeled $P45_{683}$, $P48_{683}$, and $P50_{683}$, respectively. N-terminal sequences were obtained by Edman degradation and LC-MS/MS. Sequences obtained by Edman degradation are shown in *boxes* and were taken from gel spots *circled* in *red*. Two Edman sequences from $P45_{683}$ show an intact N terminus with no signal peptide cleavage. The N terminus of $P48_{683}$ was identified using LC-MS/MS (shown in *blue*). Mass spectrum of this fragment shows an N-terminal pyroglutamate, derived from the original glutamine, which blocks the free N terminus and explains the failure of Edman degradation for this fragment (supplemental Fig. 1). *B,* molecular analysis of *mhp683*. For PONDR VSL1 analysis (*top*), regions *above the line* at 0.5 denote disordered regions within Mhp683. *Thick bars* denote disordered regions spanning 40 or more amino acids (55). Mhp683 is predicted to contain three regions of significant disorder, two corresponding with the cleavage sites of Mhp683. The TMHMM algorithm predicts that Mhp683 contains a transmembrane domain ($p = 0.973$). Multiple coiled-coil prediction algorithms identified an EKQ repeat region as a putative coiled coil. A serine/threonine-rich region has also been identified at the C terminus of cleavage fragment $P48_{683}$. Experimentally determined cleavage site positions are also shown.

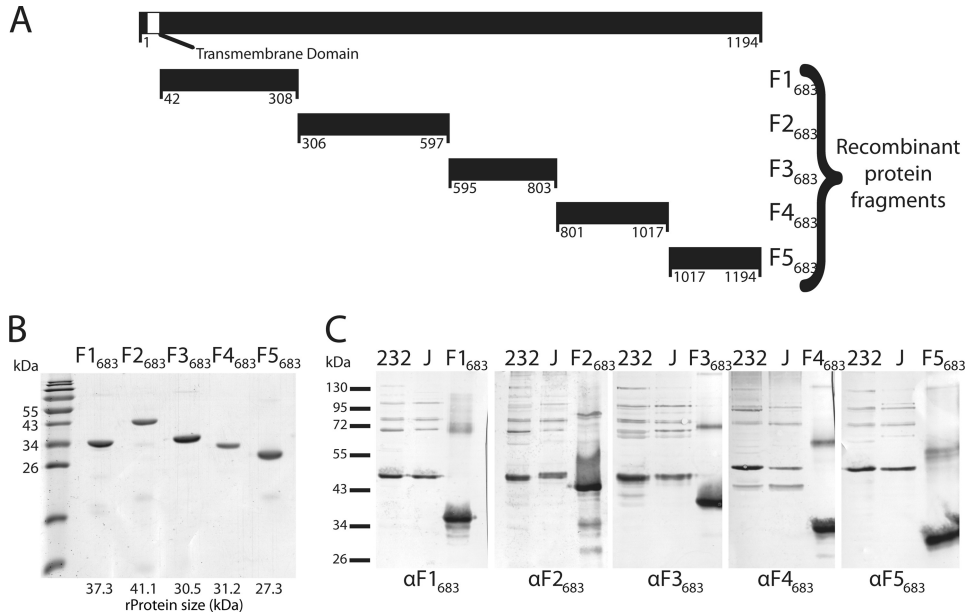

FIGURE 3. **Cloning of *mhp683* and immunoblot analysis of its protein fragments.** *A, mhp*683 (3582 bp encoding 1194 amino acids) was cloned from *M. hyopneumoniae* strain 232 as five fragments with sizes ranging from 178 to 292 amino acids. The hydrophobic putative transmembrane domain (41 amino acids) was removed from the N terminus of $F1_{683}$. All in-frame TGA codons were mutated to TGG by using either mutated flanking primers or site-directed mutagenesis. *B,* Coomassie-stained SDS-PAGE of the five recombinant protein fragments in ascending order. Recombinant protein $F3_{683}$ runs at a slightly higher molecular mass than expected on SDS-PAGE, and $F1_{683}$ runs slightly lower. *C,* immunoblots of *M. hyopneumoniae* strain 232 and J whole cell lysates, and recombinant protein fragments ($F1_{683}$–$F5_{683}$) were probed with their respective antisera ($\alpha F1_{683}$–$\alpha F5_{683}$).

between 5 and 6 and molecular mass of ~48 kDa. A linear array of five protein spots resolving at pI 7–9 and with a mass of ~50 kDa mapped to the C terminus of Mhp683 ($P50_{683}$; Fig. 2*A*). A peptide (^{1}MNQFDEKEK^{9}) was identified that spanned the first nine amino acids from the putative N-terminal methionine residue indicating that $P45_{683}$ includes the N terminus of Mhp683. This was confirmed by Edman sequencing of proteins from two spots representing $P45_{683}$ (Fig. 2*A, circled* in *red*) that generated the sequence ^{1}MNQFDEKEKQHNKAKAIL^{18}. Edman sequencing of protein spots that generated tryptic peptides spanning amino acids 773–1201 ($P50_{683}$) produced the sequence ^{755}QEQEKQQVKEQKQKQEKT^{772} indicating that the cleavage site that creates $P50_{683}$ resides between Phe-754 and Gln-755.

We were unsuccessful in attempts to determine the N-terminal sequence of $P48_{683}$ by Edman degradation. Peptide mass fingerprinting analyses of protein spots containing $P48_{683}$ indicated that the $P45_{683}$/$P48_{683}$ cleavage site is situated in the region spanning two lysine residues at positions 392 and 423 in Mhp683. To identify the N terminus of $P48_{683}$, tryptic digests of spots representing $P48_{683}$ were subjected to LC-MS/MS. This analysis identified a 21-residue semi-tryptic peptide ^{403}Q(−17)EEDLKNEPNSN(+1)GSEQDSFEK^{423} in spot variants of J and 232 lysates representing $P48_{683}$ (Fig. 2*A*; supplemental Fig. 1) and defined the N terminus of $P48_{683}$. The alteration of the N-terminal glutamine to pyroglutamate (−17 Da) is consistent with our inability to sequence the N terminus of $P48_{683}$ by Edman degradation (50). Our data indicate that $P50_{683}$ and $P48_{683}$ are released from the Mhp683 pre-protein by a protease that recognizes the motif TTKF ↓ QE, with cleavage occurring immediately after the phenylalanine residue. Based on this hypothesis, $P45_{683}$ spans amino acids 1–402 generating a cleavage fragment with a predicted mass of 46 kDa (pI = 8.3); $P48_{683}$ spans amino acids 403–754 with a predicted mass of 39 kDa (pI = 5.9), and $P50_{683}$ spans amino acids 755–1201 with a predicted mass of 50 kDa (pI = 7.9). Compared with $P45_{683}$ and $P50_{683}$, $P48_{683}$ is rich in glutamic acid residues, and this is likely to contribute to $P48_{683}$ resolving at a pI of 5.9 and showing abnormal migration during SDS-PAGE (Figs. 1–3) (51).

Molecular Analysis of Mhp683—Apart from the previously reported similarity with other members of the P102 family (24), BLASTP identified LppT (expect = 2e-04), the operon partner of the LppS adhesin from *Mycoplasma conjunctivae* (52, 53) as the molecule with the greatest degree of similarity to Mhp683. Sequence similarity was confined to ~350 residues of the N terminus. Examination of the remaining ~850 residues of the Mhp683 sequence, which encompasses both $P48_{683}$ and $P50_{683}$, showed no significant similarity to other proteins. These data show that endoproteolysis generates protein fragments with completely novel sequence on the surface of *M. hyopneumoniae*.

Analysis of Mhp683 with several coiled-coil prediction algorithms identified a 30-residue putative coiled-coil region between residues 742 and 776 in *M. hyopneumoniae* strain 232 and 756–785 in strain J (Fig. 2*B*). These regions correspond with an EKQ repeat domain with the motif ((QK))(EQ)(QK)(*X*) identified previously (54), which is in close proximity to the N terminus of $P50_{683}$. The COILS2 algorithm ($p > 0.9$) and the Paircoil2 algorithm ($p = 0.0243$, coiled-coil cutoff of $p < 0.025$) both indicated that the EKQ region forms a coiled coil.

The PONDR VSL1 algorithm was used to predict regions of structural disorder present within Mhp683 (Fig. 2*B*). Four areas of significant structural disorder spanning more than 40 amino acids were predicted to occur at residues 381–428, 636–777, 875–987, and 990–1084 in the strain 232 homolog (55). Similar regions were identified in the strain J homolog MHJ_0662. The

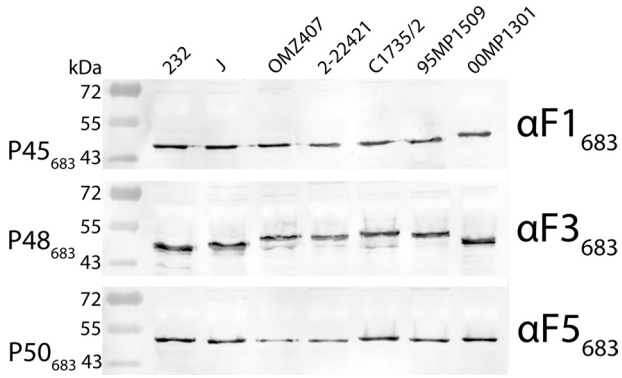

FIGURE 4. **Processing of Mhp683 homologs is conserved across geographically diverse strains of *M. hyopneumoniae*.** Immunoblots containing whole cell lysates of different *M. hyopneumoniae* field isolates were separately probed with $\alpha F1_{683}$, $\alpha F3_{683}$, and $\alpha F5_{683}$ sera to assess the consistency of protein expression and processing. Cleavage fragments equivalent to $P45_{683}$, $P48_{683}$, and $P50_{683}$ are conserved across all isolates.

predicted cleavage motif (TTKF ↓ QE) at positions 402–403 and 749–750 resided within disordered regions spanning residues 381–428 and 636–777. An S/T-rich repeat region in the C terminus of $P48_{683}$ also lies within a disordered region spanning residues 636–777 (Fig. 2*B*).

Mhp683 Is Processed in Strains with Different Geographic Origins—To determine whether Mhp683 is subject to proteolytic processing in field strains of *M. hyopneumoniae* from geographically diverse locations, immunoblots (Fig. 4) of whole cell lysates of strains sourced from Australia and the United States were probed with antisera raised against recombinant fragments $F1_{683}$–$F5_{683}$. Using $\alpha F1_{683}$, $\alpha F3_{683}$, and $\alpha F5_{683}$ sera, fragments $P45_{683}$, $P48_{683}$, and $P50_{683}$ were detected in all strains examined.

$P45_{683}$, $P48_{683}$, and $P50_{683}$ Reside on the Surface of M. hyopneumoniae—To determine whether $P45_{683}$, $P48_{683}$, and $P50_{683}$ reside on the surface of *M. hyopneumoniae*, immunoblots containing cell lysates of freshly cultured cells that have been exposed to different concentrations of trypsin for 15 min (37 °C) were separately probed with $\alpha F1_{683}$, $\alpha F3_{683}$, and $\alpha F5_{683}$ sera detecting cleavage fragments $P45_{683}$, $P48_{683}$, and $P50_{683}$, respectively (Fig. 5*A*). These protein bands were almost completely digested at a trypsin concentration of 50 μg ml^{-1}. Identical lysates exposed to antisera raised against the ribosomal protein L7/L12 showed that this protein was detected at a trypsin concentration of 300 μg ml^{-1} suggesting that the integrity of cell membrane remained unaffected in these experiments. In addition to immunoblotting, we combined trypsin digestion of whole cell *M. hyopneumoniae* with mass spectrometry. After digestion, multiple peptides unique to cleavage fragments $P45_{683}$, $P48_{683}$, and $P50_{683}$ were identified by LC-MS/MS (supplemental Fig. 2).

To further confirm surface localization, we biotinylated intact *M. hyopneumoniae* cells, purified biotin-conjugated proteins, and examined them using two-dimensional electrophoresis and LC-MS/MS. Peptides unique to $P45_{683}$, $P48_{683}$, and $P50_{683}$ were each identified at masses similar to those determined in previous electrophoresis experiments (Fig. 5*B*). Biotinylation of each protein spot was confirmed by matching to a streptavidin blot prepared from a simultaneously run two-dimensional gel. We identified a 10-residue semi-tryptic peptide with sequence ^{393}VDNNTSTTKF^{402} that defines the C terminus of $P45_{683}$ and provides further evidence of cleavage at the TTFK ↓ QE motif (supplemental Fig. 3).

Predicting Cleavage Sites in Other Members of the P97 Family of Paralogs—Previously, we showed that the cilium adhesin Mhp493 and its homolog in strain J (MHJ_0493) was subject to a major cleavage event that removes 85 kDa from the C terminus of the 216-kDa pre-protein. Attempts to delineate the N terminus of P85 by Edman degradation were unsuccessful (15). Peptide mass fingerprinting indicated that the N terminus of P85 resided between amino acids 1041 and 1089 in Mhp493 (15). Based on the reiterated cleavage site TTKF ↓ QE identified in this study, we hypothesized that the sequence STNF ↓ QE, which also resides in a strongly disordered region of Mhp493, may be recognized by the same putative protease that cleaves Mhp683. A semi-tryptic fragment with the sequence ^{1075}QEEADLDQDGQDDSR^{1089} was identified by LC-MS/MS and defines the N terminus of P85 (Fig. 6; supplemental Fig. 4).

Mhp683 Binds Heparin—In previous studies we have identified members of the P97 family as heparin-binding proteins (15, 16, 18, 48). To determine whether Mhp683 binds glycosaminoglycans, we performed microtiter plate assays with biotin-labeled heparin. Recombinant fragments $F1_{683}$–$F5_{683}$ spanning Mhp683 bound to biotinylated heparin in a dose-dependent and saturable manner (Fig. 7*A*). Binding was almost completely inhibited by the presence of a large excess of unlabeled heparin indicating that the binding interaction was specific. Recombinant protein $F4_{683}$ bound heparin with the highest affinity (K_d = 19.63 ± 1.75 nM) and $F1_{683}$ bound with lowest affinity (K_d = 123.8 ± 23.8 nM). Unlabeled heparin and fucoidan were found to effectively inhibit the binding of biotinylated heparin to all recombinant fragments, whereas chondroitin sulfates A and B did not (Fig. 7*B*). The ability of porcine mucin II to inhibit heparin binding varied for each recombinant fragment. Mucin dramatically inhibited the ability of $F1_{683}$ to bind heparin. Mucin also inhibited the binding of heparin to $F2_{683}$ and $F5_{683}$, but it only had a moderate effect on the ability of $F3_{683}$ to bind heparin. Mucin did not significantly inhibit $F4_{683}$ from binding heparin. The heparin binding observed in microtiter plate assays were largely consistent when examined using dot-blot ligand binding assays with the recombinants bound to nitrocellulose in a native conformation (Fig. 7*C*). $F4_{683}$ was again found to have the highest affinity for biotinylated heparin, whereas $F2_{683}$ displayed the least affinity. The affinity of $F1_{683}$ for heparin was higher compared with the microtiter plate assays. $F1_{683}$, $F2_{683}$, and $F5_{683}$ completely lost affinity for biotinylated heparin when applied to the membrane after denaturation, and the affinity to $F3_{683}$ was significantly weakened (Fig. 7*D*). $F4_{683}$ retained its ability to bind biotinylated heparin regardless of its conformational state.

Mhp683 Binds Porcine Cilia—A microtiter plate assay used previously to identify cilium-binding proteins (15) showed that Mhp683 recombinant proteins $F1_{683}$–$F5_{683}$ reproducibly bind cilia. The recombinant protein $F1_{216}$, previously reported to display low cilium binding properties (15), did not bind porcine cilia. $F2_{P97}$, a recombinant protein that carries the R1 cilium

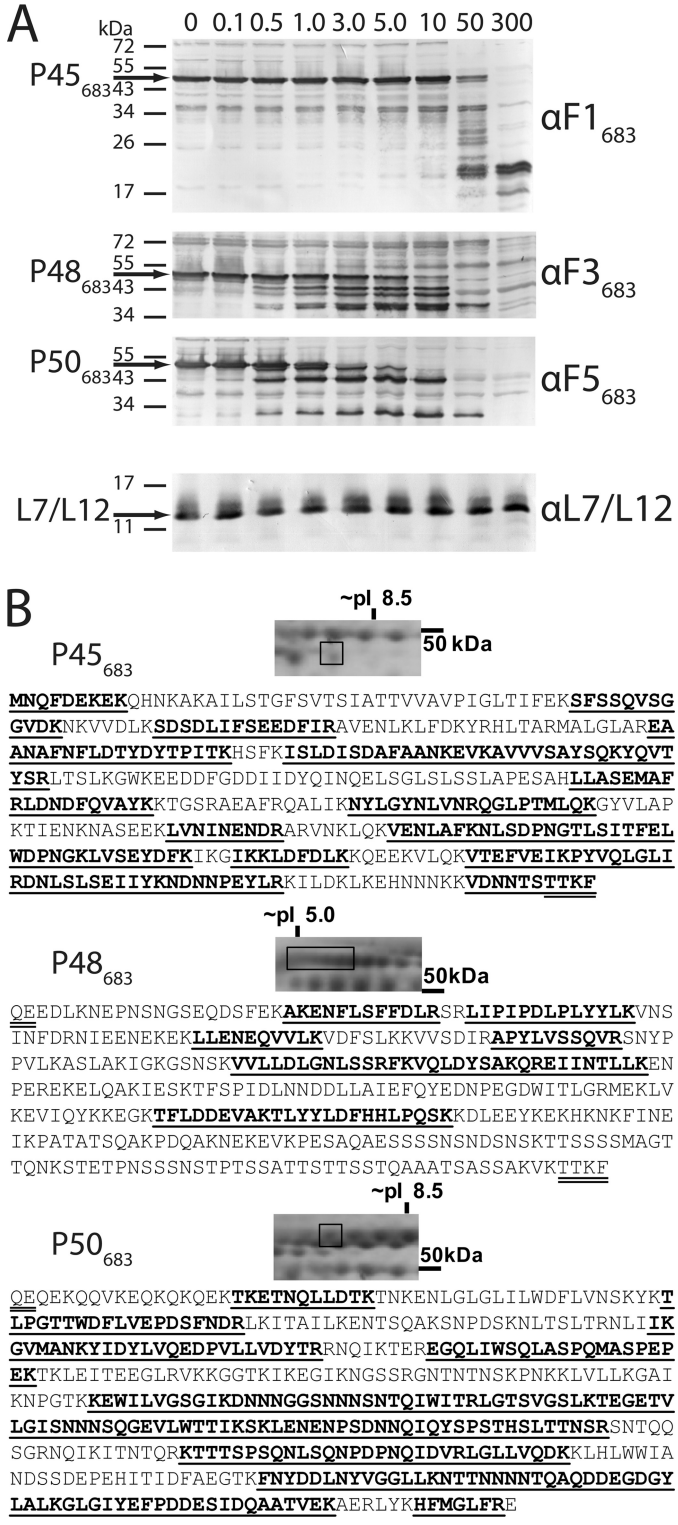

FIGURE 5. **MHJ_0662 (Mhp683 homolog) is present on the surface of *M. hyopneumoniae*.** *A,* intact and washed (strain J) cells were digested for 15 min with increasing concentrations of trypsin to determine whether $P45_{683}$, $P48_{683}$, and $P50_{683}$ fragments were present on the cell surface. Immunoblots were probed with $\alpha F1_{683}$, $\alpha F3_{683}$, and $\alpha F5_{683}$ sera and identified $P45_{683}$, $P48_{683}$, and $P50_{683}$ fragments of MHJ_0662, respectively. Trypsin concentrations (*above blots*) are quoted in $\mu g\ ml^{-1}$. Identical lysates were subsequently probed with antiserum to an intracellular control protein (ribosomal protein L7/L12) to confirm cellular integrity. *B,* surface biotinylation of *M. hyopneumoniae*. Intact and washed *M. hyopneumoniae* (strain J) cells were biotinylated and lysed, and biotin conjugates were purified by affinity chromatography. Following separation by two-dimensional electrophoresis, peptides unique to $P45_{683}$, $P48_{683}$, and $P50_{683}$ were identified from purified biotinylated proteins by LC-MS/MS. *Underlined sequences* indicate peptides identified by LC-MS/MS; *M. hyopneumoniae* cleavage site motifs are *double underlined*.

binding domain of cilium adhesin P97, was used as a positive control and bound to porcine cilia as expected (Fig. 8*A*).

Mhp683 Antibodies Inhibit Adherence of M. hyopneumoniae to Cilia—Antibodies that bind the R1 region of the cilium adhesin P97 have been previously shown to block the adherence of *M. hyopneumoniae* to porcine cilia (20). To determine whether this was the case with Mhp683 antibodies, we incubated *M. hyopneumoniae* with $\alpha F1_{683}$–$\alpha F5_{683}$ sera and examined binding to porcine cilia in a microtiter-based assay. *M. hyopneumoniae* binding to porcine cilia was significantly and reproducibly inhibited by both $\alpha F2_{683}$ and $\alpha F5_{683}$ sera (Fig. 8*B*). Binding of *M. hyopneumoniae* coated in $\alpha F2_{683}$ and $\alpha F5_{683}$ sera was reduced by 52.0 ± 6.1% and 39.5 ± 7.5%, respectively. Binding of *M. hyopneumoniae* to cilia was not significantly inhibited by treatment with $\alpha F1_{683}$, $\alpha F3_{683}$, or $\alpha F4_{683}$ sera. The adherence blocking control, $\alpha F2_{P97}$, an antiserum recognizing the R1 cilium binding domain of cilium adhesin P97, was also used and inhibited *M. hyopneumoniae* binding to porcine cilia by 63.1 ± 3.3% consistent with previously reported observations (20).

DISCUSSION

mhp683, the second gene in a putative two-gene operon with *mhp684*, encodes a protein with a predicted mass of 135 kDa, but a protein with this mass and a tryptic cleavage pattern matching to Mhp683 was not found when high mass proteins resolved by SDS-PAGE were characterized by MALDI-TOF MS (15). Data from SDS-PAGE and LC-MS/MS and two-dimensional immunoblotting using sera raised against recombinant fragments spanning Mhp683 provide strong evidence that Mhp683 and homologs in strains of *M. hyopneumoniae* from geographically diverse regions are subject to two post-translational cleavage events that produce proteins $P45_{683}$, $P48_{683}$, and $P50_{683}$. Trypsin digestion and surface biotinylation experiments show that $P45_{683}$, $P48_{683}$ and $P50_{683}$ reside on the surface of *M. hyopneumoniae*, suggesting that in the absence of membrane spanning domains, the fragments must bind to other surface-localized components of either *Mycoplasma* or host origin. Recombinant proteins ($F1_{683}$–$F5_{683}$) spanning Mhp683 bind heparin and porcine cilia suggesting that $P45_{683}$, $P48_{683}$, and $P50_{683}$ each play an important role in facilitating colonization of the respiratory tract of swine.

During broth culture, the P97 and P102 paralogs are among the most highly expressed proteins,[3] and mRNAs derived from genes that encode these proteins have been detected in *M. hyopneumoniae* recovered from the lungs of infected swine (12). We have previously established that proteolytic processing of members of the P97 and P102 paralog families generates a complex array of cleavage fragments that are displayed on the surface of *M. hyopneumoniae* and perform key roles in adhesion to structurally diverse host molecules (13–18, 48). However, the rationale for the extensive proteolytic processing of these

[3] M. P. Padula and S. P. Djordjevic, unpublished data.

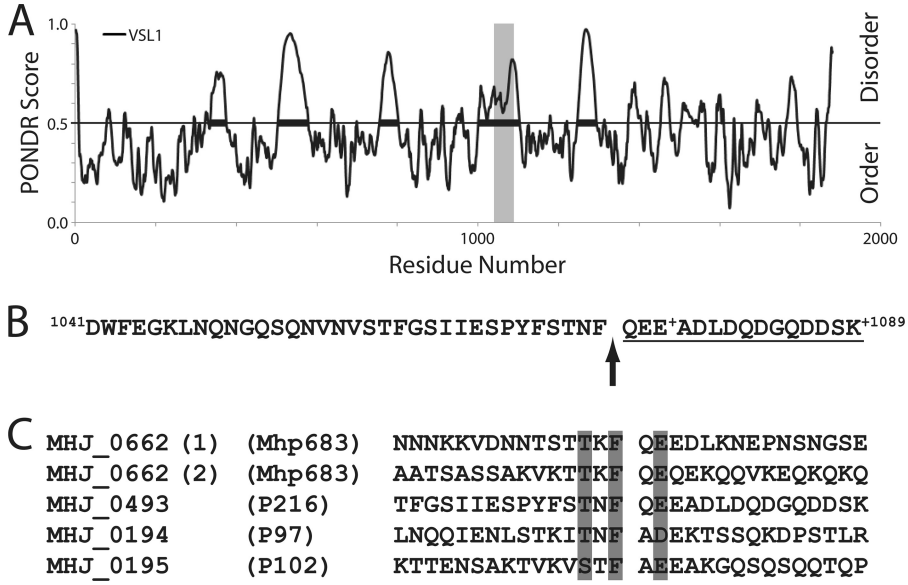

FIGURE 6. **Peptide motif TTKFQE found in Mhp683 is predictive of other cleavage sites within the P97/P102 family; identification of the Mhp493 cleavage site.** *A,* PONDR analysis of Mhp493 (P216). Cleavage of Mhp493 into P120 and P85 was previously identified, but the precise cleavage site was unable to be accurately determined (15). *Gray bar* denotes region spanning amino acids 1041–1089 previously shown to house the putative cleavage site. *B,* amino acids 1041–1089 of the strain J homolog (MHJ_0493) of Mhp493. The N-terminal peptide identified by LC-MS/MS (supplemental Fig. 4) is *underlined*. *Arrow* denotes the site of cleavage that separates 85 kDa (P85) from the C terminus of MHJ_0493. + identifies a site of amino acid variability. The comparable sequence in Mhp493 from strain 232 is identical except an aspartic acid residue replaces a glutamic acid residue at position 1077 and an asparagine residue replaces a lysine residue at position 1089. *C,* comparison of identified P97/P102 family cleavage sites (14). *Shaded regions* denote highly similar or identical residues.

adhesins by *M. hyopneumoniae* remains elusive. The respiratory pathogen *Bordetella pertussis* also proteolytically cleaves its FHA adhesin, and although mutants lacking the responsible protease (SphB1) retained respiratory cell adhesion, they had a decreased ability to colonize lung tissue (56). This suggested that processing of FHA facilitated the detachment of individual bacteria from microcolonies, allowing infection to efficiently spread within the host (56). Adhesin processing in *M. hyopneumoniae* may have a similar role; unfortunately, due to the present absence of a targeted gene knock-out technique for this bacterium, this hypothesis cannot be tested using this approach.

Although considerable progress has been made in determining the precise cleavage sites for a number of proteolytic cleavage events (13, 14), attempts to define the N-terminal sequences of a number of cleavage products have failed (13, 15) presumably due to chemical modifications to N-terminal residues that block Edman degradation. Here, we identify a reiterated cleavage motif with sequence TTKF ↓ QE in Mhp683. Cleavage after the phenylalanine residue was confirmed by a combination of Edman sequencing of $P50_{683}$ and LC-MS/MS of both the $P48_{683}$ N terminus and $P45_{683}$ C terminus. The semi-tryptic peptide ^{403}Q(−17)EEDLKNEPNSN(+1)GSEQDSFEK^{423}, where −17 denotes the presence of pyroglutamate and +1 the conversion of asparagine to aspartic acid through deamidation (57), was identified on numerous occasions by mass spectrometry and defined the N terminus of $P48_{683}$. Previous attempts to perform Edman degradation on $P48_{683}$ were unsuccessful presumably due to the presence of pyroglutamate, which is known to block Edman sequencing (50). Further evidence for cleavage at this position was provided by the identification of the semi-tryptic peptide, ^{393}VDNNTSTTKF^{402} representing the C terminus of $P45_{683}$.

Although unsuccessful in previous attempts to accurately define cleavage sites within the P97 paralog Mhp493 (15) and in the P102-related molecule Mhp494 (13) by Edman sequencing, we were able to accurately localize the cleavage site to within short stretches of sequence using peptide mapping strategies. We hypothesized that the identification of the reiterated cleavage sequence TTKF ↓ QE in Mhp683 may facilitate accurate prediction of cleavage sites within other P97 and P102 paralogs. To test this hypothesis, we selected the P97 paralog Mhp493 (P216). Mhp493 undergoes a cleavage event generating fragments P120 and P85 (15), which display cilium binding properties on the surface of *M. hyopneumoniae*. Peptide mapping analyses delineated the N terminus to reside within a stretch of 49 amino acids spanning positions 1041 to 1089. A sequence ^{1071}STNF ↓ QE^{1076} identified in this region of Mhp493 closely resembled the TTKF ↓ QE cleavage motif in Mhp683. A semi-tryptic peptide with the sequence ^{1075}QEEADLDQDGQDDSR^{1089} was identified by LC-MS/MS, which defined the N terminus of P85. Interestingly, the two TTKF ↓ QE cleavage sites and the STNF ↓ QE cleavage site each reside within intrinsically disordered regions (Figs. 2 and 6) in Mhp683 and Mhp493, respectively. Regions within proteins displaying intrinsic disorder are often targets for proteolytic attack and other post-translational modifications (55, 58). These data suggest that a protease in *M. hyopneumoniae* responsible for processing the P97 and P102 family of cilium adhesins recognizes a peptide motif with a sequence similar to TTKF ↓ QE.

We have previously identified several cleavage sites within P97 and P102 by Edman sequencing (14, 20). Analysis of the

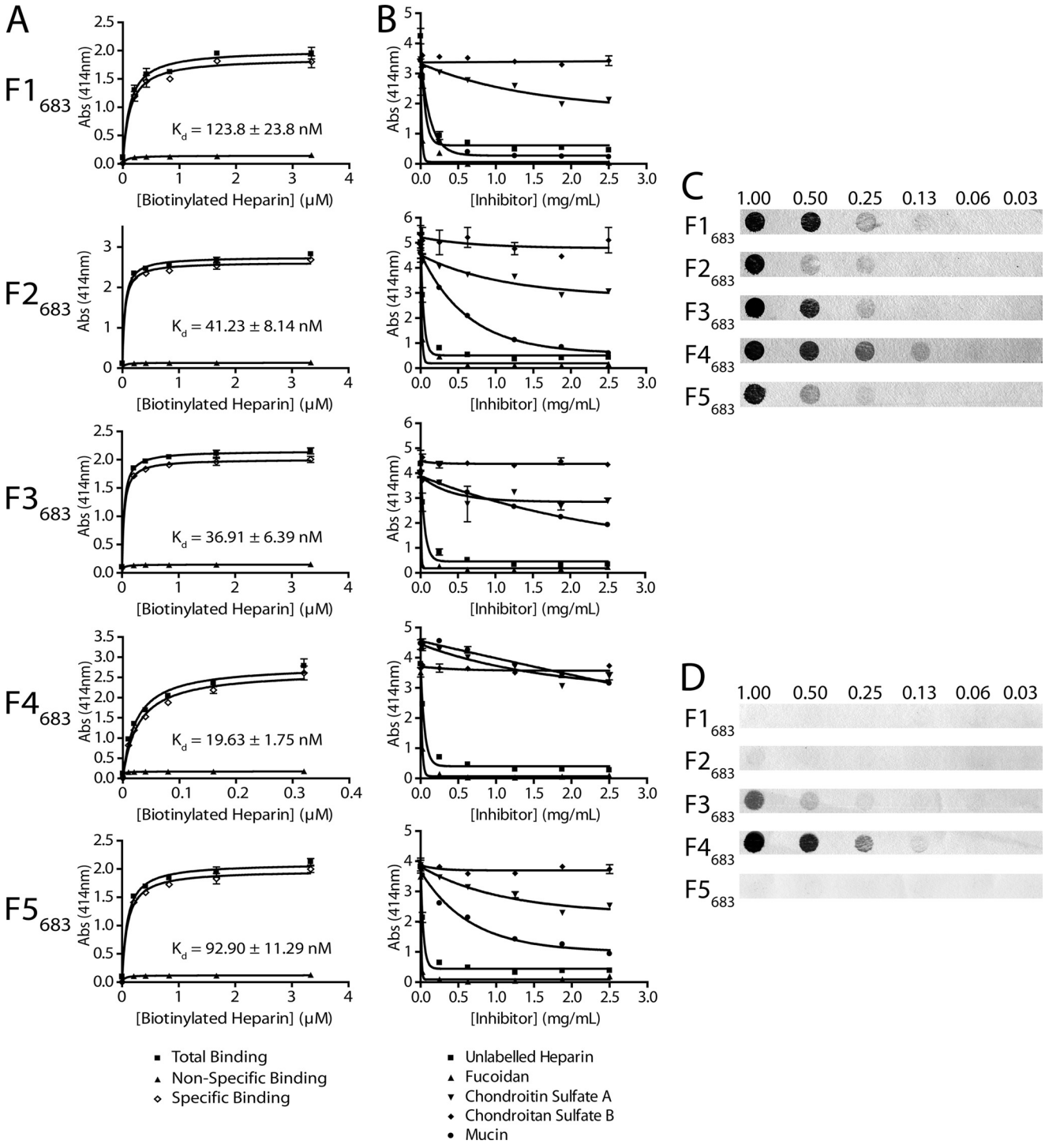

FIGURE 7. **Recombinant proteins $F1_{683}$–$F5_{683}$ bind heparin.** *A,* binding of recombinant protein to biotinylated heparin. Total binding (■) was determined by coating recombinant protein $F1_{683}$–$F5_{683}$ (10 μg ml^{-1}) to 96-well microtiter plates followed by binding with increasing concentrations of biotinylated heparin (*x* axis). Nonspecific binding (▲) was determined by binding with unlabeled heparin in a 50-fold excess to biotinylated heparin. Specific binding (◇) was determined by subtracting the nonspecific from the total binding. K_d values for all five recombinant proteins were determined from the specific binding data. *B,* inhibition of heparin binding by glycosaminoglycans. Recombinant protein (10 μg ml^{-1}) was coated to 96-well microtiter plates and bound with biotinylated heparin in the presence of an increasing excess of inhibitor (*x* axis). Inhibitors included unlabeled heparin (■), fucoidan (▲), chondroitin sulfate A (▼), chondroitin sulfate B (♦), and porcine type II mucin (●). *C,* nondenatured recombinant protein dot blots. Recombinant proteins were spotted onto nitrocellulose membrane, blocked, and incubated with 30 μg ml^{-1} biotinylated heparin. Bound recombinant protein amounts (*above blots*) are listed in micrograms. *D,* denatured recombinant protein dot blots. Recombinant proteins were denatured by boiling in an SDS-containing reducing solution before spotting onto nitrocellulose membrane and incubation with heparin as with *C*. Bound recombinant protein amounts (above blots) are listed in micrograms.

sequences surrounding these cleavage sites reveals two motifs that closely resemble those we have identified in this study (Fig. 6*C*). The sequence ^{192}ITNF ↓ AD^{197} in Mhp183 spans the cleavage site responsible for the maturation of the cilium adhesin P97. This cleavage event removes 195 amino acids from the N terminus of the 125-kDa pre-protein (Mhp183), generating

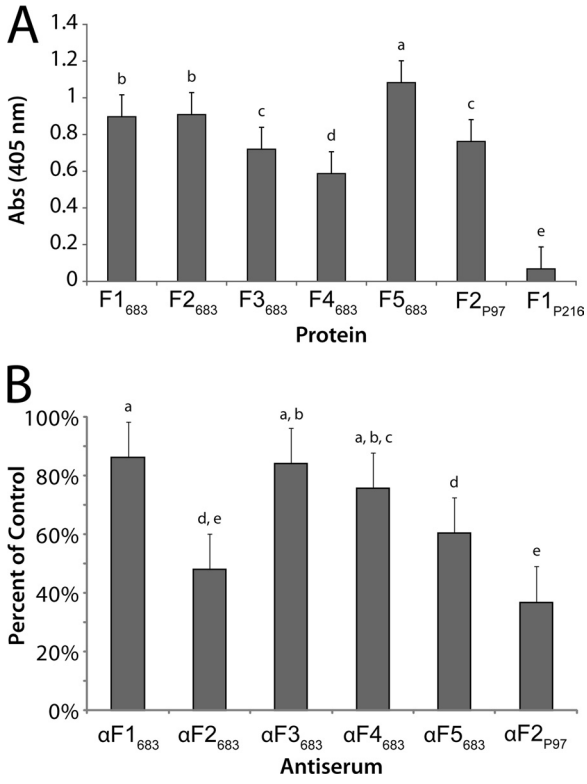

FIGURE 8. **Mhp683 recombinant proteins bind porcine cilia, and antisera blocks cilium binding by *M. hyopneumoniae*.** *A,* cilium binding assay. Microtiter plate binding assay showing Mhp683 recombinant fragments binding to porcine cilia. Recombinant fragment derived from P97 encoding the cilium binding domain R1 and R2 ($F2_{P97}$) acted as a positive control for cilium binding in this experiment (48). The recombinant fragment that has previously been reported to have low cilium binding ($F1_{P216}$) acted as a negative control for cilium binding in this experiment (15). Data represent means plus least significant difference at $p < 0.05$. Means with any superscript (*a–e*) in common are not different; those with no superscript in common are different at $p < 0.05$. *B, M. hyopneumoniae* adherence to porcine cilia is blocked by Mhp683 antisera. Microtiter plate assay showing inhibition of *M. hyopneumoniae* binding to porcine cilia after pretreatment with $\alpha F1_{683}$–$\alpha F5_{683}$ sera diluted at 1:50. Data are presented as a percentage of binding control, where cells were incubated in rabbit sera with no specificity to *M. hyopneumoniae* proteins. Antisera ($\alpha F2_{P97}$) derived from the recombinant fragment $F2_{P97}$ was used as a blocking control. Data represent means plus least significant difference at $p < 0.05$. Means with any superscript (*a–e*) in common are not different; those with no superscript in common are different at $p < 0.05$. Binding control (100%) was in statistical group *a*.

the mature P97 adhesin and the N-terminal cleavage product P22 (14, 20, 59). The sequence ^{553}VSTF ↓ AE^{558} spans the cleavage site in Mhp182 (P102) that generates the N-terminal 72-kDa fragment (P72) and the C-terminal 42-kDa fragment (P42) (14). Comparison of these cleavage motifs with those of this study identifies three key features as follows: (i) the amino side residue of the cleavage site (−1 position) is phenylalanine; (ii) the −3 position (amino cleavage fragment) is an alcohol-containing residue (S/T); (iii) the +2 position (carboxyl cleavage fragment) is negatively charged (D/E) (Fig. 6*C*). Our data suggest that a putative protease(s) responsible for processing in *M. hyopneumoniae* recognizes some or all of these key residues. The characterization of further N-terminal sequences either by Edman degradation or mass spectrometry would facilitate the definition of a robust protease recognition motif, which would be valuable in the global prediction of proteolytic cleavage sites from *M. hyopneumoniae* genome sequences.

Primary bacterial pathogens are capable of overcoming the protective effects of the mucosal barrier and colonize epithelial sites in the respiratory tract. These processes expose previously inaccessible colonization sites that provide opportunities for secondary bacterial pathogens to exploit (60). The identification and characterization of the molecules involved in the adherence to both cilia and extracellular matrix components are important first steps in understanding the pathogenic armory of *M. hyopneumoniae*. Epithelial surfaces are awash with mucins, antimicrobial peptides, and mucopolysaccharides that act as decoys for microbial adhesins (60). Glycosaminoglycans are present in the extracellular matrix and include regions of proteoglycans that are exposed on the surface of almost all eukaryotic cells (61). Heparan sulfate, an important component of proteoglycans, has been identified on the cilial surface in the swine upper respiratory tract (21). In other bacterial pathogens, heparan sulfate has been identified as a key target for adhesive proteins that either bind directly or via recruitment of other glycosaminoglycan-binding host molecules (62–64). In *M. hyopneumoniae*, we have previously identified a number of glycosaminoglycan-binding proteins from the P97 family (13, 15, 16, 18, 48). Here, we show that recombinant fragments $F1_{683}$–$F5_{683}$ of Mhp683 bind heparin at physiologically significant levels in a saturable and dose-dependent manner. Heparin is structurally analogous to the sulfated regions of heparan sulfate found on the surfaces of epithelial cells and is a reliable substrate for the identification of glycosaminoglycan-binding proteins (65). Because of the high negative charge of heparin, interactions with bacterial adhesins are largely mediated via lysine and arginine residues, although polar amino acids such as asparagine and glutamine also contribute (66). The loss of binding due to denaturation of $F1_{683}$, $F2_{683}$, $F3_{683}$, and $F5_{683}$ indicates that adherence to heparin was largely dependent on conformational epitopes. $F4_{683}$, however, retained an ability to bind heparin after boiling in Laemmli buffer indicating that a linear heparin-binding motif may be present in this sequence. Analysis of the isoelectric points of the $F1_{683}$–$F5_{683}$ indicates that $F4_{683}$ is the most alkaline with a theoretical pI of 9.70. Arginine and lysine make up 15% of the total amino acid complement of $F4_{683}$ and are likely to play an important role in binding heparin.

Competitive binding assays showed that the ability of $F1_{683}$–$F5_{683}$ to bind heparin was effectively inhibited by fucoidan but not significantly by chondroitin sulfate A or B, indicating that the presence and placement of sulfate functional groups are important (48, 65). Porcine mucin also inhibited the ability of $F1_{683}$, $F2_{683}$, and $F5_{683}$ and to a lesser extent $F3_{683}$ to bind heparin, but this effect was not observed with heparin binding to $F4_{683}$. These data suggest heparin binding domains are scattered throughout Mhp683 and that all three cleavage fragments $P45_{683}$, $P48_{683}$, and $P50_{683}$ bind proteoglycans and play important roles in colonizing mucosal epithelial cilia.

P97 uses variable tandem repeat regions to facilitate adherence to both cilia and extracellular matrix components. The R1 and R2 regions of P97 and Mhp271 have both been identified as key sequences involved in the binding of cilia and heparin (16, 48, 67). Mhp683 possesses a variable tandem repeat region rich in EKQ residues (54). Our results suggest that it is not critical in facilitating binding of Mhp683 to either heparin or cilia. The

EKQ region includes a KEKE-like motif that has been implicated in protein-protein interactions (68–70). Analysis of other P97/P102 paralogs demonstrates that this motif is present in Mhp684 (P146 adhesin-like protein), Mhp493 (P216), and Mhp494 (P159 adhesin). KEKE motifs are often associated with a coiled-coil protein structure (70), and the EKQ region in Mhp683 is predicted to display a coiled-coil conformation. Coiled-coil regions are associated with adhesins such as the Vaa adhesin of *Mycoplasma hominis* (71). The function of putative coiled-coil regions in *M. hyopneumoniae* surface proteins remains unknown.

Mhp683 is one of a growing number (Mhp493, Mhp107, and Mhp108) of cilial adhesins of *M. hyopneumoniae* that do not display an R1 cilium binding domain. In this study, recombinant fragments $F1_{683}$–$F5_{683}$ were observed to bind porcine cilia in a microtiter-based assay previously used to identify the P97 adhesin. Critically, we have also demonstrated that antisera to Mhp683 recombinant proteins significantly and reproducibly inhibited the adherence of *M. hyopneumoniae* to porcine cilia underlining the biological importance of this protein to the bacterium. Both $\alpha F2_{683}$ and $\alpha F5_{683}$ sera significantly blocked this interaction, and inhibition by $\alpha F2_{683}$ was observed at levels similar to antiserum made from a recombinant protein containing the R1 binding domain of the cilium adhesin P97. Inhibition of *M. hyopneumoniae* adherence to porcine cilia was not absolute as ~50% of *Mycoplasma* cells were able to bind cilia after coating with Mhp683 antisera, a result consistent with the redundancy previously observed in the P97 and P102 families (15–18, 20). Although $\alpha F2_{683}$ and $\alpha F5_{683}$ sera significantly inhibited binding of *M. hyopneumoniae* to porcine cilia; antisera to recombinant fragments $F1_{683}$, $F3_{683}$, and $F4_{683}$ did not, despite evidence that they directly bound porcine cilia, indicating that $F2_{683}$ and $F5_{683}$ contain critical and exposed binding sites that play significant roles in *M. hyopneumoniae* pathogenesis.

Our analysis of members of the P97 and P102 families show that they are highly expressed, subject to proteolytic cleavage and other post-translational modification events, and often display unusual sequence motifs (13–18). Although we do not understand how adhesin cleavage fragments remain attached to the cell surface, the identification of a proteolytic cleavage motif represents a significant development that should facilitate the prediction of other processed surface proteins and their cleavage sites and assist in the identification of the putative protease(s). The growing number of surface proteins dedicated to binding epithelial cilia attests to the importance colonization of this niche plays in the survival, proliferation, and spread of this ubiquitous and economically important pathogen. It is clear that proteolytic cleavage fragments derived from Mhp683 and other members of the P97 and P102 families are critical components of the surface architecture of *M. hyopneumoniae*.

Acknowledgments—We thank Ben Crossett for the preliminary matrix-assisted laser desorption/ionization-time-of-flight MS work done to locate Mhp683 and David C. Oneal for original mutagenesis work on mhp683.

REFERENCES

1. Clark, L., Armstrong, C., Scheidt, A., and VanAlstine, W. G. (1993) *J. Swine Health Prod.* **1,** 10–14
2. Haesebrouck, F., Pasmans, F., Chiers, K., Maes, D., Ducatelle, R., and Decostere, A. (2004) *Vet. Microbiol.* **100,** 255–268
3. Chin, J., San Gil, F., Novak, M., Eamens, G., Djordjevic, S., Simecka, J., Duncan, J., and Mullbacher, A. (1996) *J. Biotechnol.* **44,** 13–19
4. Djordjevic, S. P., Eamens, G. J., Romalis, L. F., Nicholls, P. J., Taylor, V., and Chin, J. (1997) *Aust. Vet. J.* **75,** 504–511
5. Fagan, P. K., Djordjevic, S. P., Chin, J., Eamens, G. J., and Walker, M. J. (1997) *Infect. Immun.* **65,** 2502–2507
6. Fagan, P. K., Djordjevic, S. P., Eamens, G. J., Chin, J., and Walker, M. J. (1996) *Infect. Immun.* **64,** 1060–1064
7. Fagan, P. K., Walker, M. J., Chin, J., Eamens, G. J., and Djordjevic, S. P. (2001) *Microb. Pathog.* **30,** 101–110
8. Matic, J. N., Terry, T. D., Van Bockel, D., Maddocks, T., Tinworth, D., Jennings, M. P., Djordjevic, S. P., and Walker, M. J. (2009) *Infect. Immun.* **77,** 1817–1826
9. DeBey, M. C., and Ross, R. F. (1994) *Infect. Immun.* **62,** 5312–5318
10. Mebus, C. A., and Underdahl, N. R. (1977) *Am. J. Vet. Res.* **38,** 1249–1254
11. Tajima, M., and Yagihashi, T. (1982) *Infect. Immun.* **37,** 1162–1169
12. Adams, C., Pitzer, J., and Minion, F. C. (2005) *Infect. Immun.* **73,** 7784–7787
13. Burnett, T. A., Dinkla, K., Rohde, M., Chhatwal, G. S., Uphoff, C., Srivastava, M., Cordwell, S. J., Geary, S., Liao, X., Minion, F. C., Walker, M. J., and Djordjevic, S. P. (2006) *Mol. Microbiol.* **60,** 669–686
14. Djordjevic, S. P., Cordwell, S. J., Djordjevic, M. A., Wilton, J., and Minion, F. C. (2004) *Infect. Immun.* **72,** 2791–2802
15. Wilton, J., Jenkins, C., Cordwell, S. J., Falconer, L., Minion, F. C., Oneal, D. C., Djordjevic, M. A., Connolly, A., Barchia, I., Walker, M. J., and Djordjevic, S. P. (2009) *Mol. Microbiol.* **71,** 566–582
16. Deutscher, A. T., Jenkins, C., Minion, F. C., Seymour, L. M., Padula, M. P., Dixon, N. E., Walker, M. J., and Djordjevic, S. P. (2010) *Mol. Microbiol.* **78,** 444–458
17. Seymour, L. M., Deutscher, A. T., Jenkins, C., Kuit, T. A., Falconer, L., Minion, F. C., Crossett, B., Padula, M., Dixon, N. E., Djordjevic, S. P., and Walker, M. J. (2010) *J. Biol. Chem.* **285,** 33971–33978
18. Seymour, L. M., Falconer, L., Deutscher, A. T., Minion, F. C., Padula, M. P., Dixon, N. E., Djordjevic, S. P., and Walker, M. J. (2011) *J. Biol. Chem.* **286,** 10097–10104
19. Minion, F. C., Adams, C., and Hsu, T. (2000) *Infect. Immun.* **68,** 3056–3060
20. Zhang, Q., Young, T. F., and Ross, R. F. (1995) *Infect. Immun.* **63,** 1013–1019
21. Erlinger, R. (1995) *Cell Tissue Res.* **281,** 473–483
22. Zhang, Q., Young, T. F., and Ross, R. F. (1994) *Infect. Immun.* **62,** 1616–1622
23. Zielinski, G. C., Young, T., Ross, R. F., and Rosenbusch, R. F. (1990) *Am. J. Vet. Res.* **51,** 339–343
24. Minion, F. C., Lefkowitz, E. J., Madsen, M. L., Cleary, B. J., Swartzell, S. M., and Mahairas, G. G. (2004) *J. Bacteriol.* **186,** 7123–7133
25. Vasconcelos, A. T., Ferreira, H. B., Bizarro, C. V., Bonatto, S. L., Carvalho, M. O., Pinto, P. M., Almeida, D. F., Almeida, L. G., Almeida, R., Alves-Filho, L., Assunção, E. N., Azevedo, V. A., Bogo, M. R., Brigido, M. M., Brocchi, M., Burity, H. A., Camargo, A. A., Camargo, S. S., Carepo, M. S., Carraro, D. M., de Mattos Cascardo, J. C., Castro, L. A., Cavalcanti, G., Chemale, G., Collevatti, R. G., Cunha, C. W., Dallagiovanna, B., Dambrós, B. P., Dellagostin, O. A., Falcão, C., Fantinatti-Garboggini, F., Felipe, M. S., Fiorentin, L., Franco, G. R., Freitas, N. S., Frías, D., Grangeiro, T. B., Grisard, E. C., Guimarães, C. T., Hungria, M., Jardim, S. N., Krieger, M. A., Laurino, J. P., Lima, L. F., Lopes, M. I., Loreto, E. L., Madeira, H. M., Manfio, G. P., Maranhão, A. Q., Martinkovics, C. T., Medeiros, S. R., Moreira, M. A., Neiva, M., Ramalho-Neto, C. E., Nicolás, M. F., Oliveira, S. C., Paixão, R. F., Pedrosa, F. O., Pena, S. D., Pereira, M., Pereira-Ferrari, L., Piffer, I., Pinto, L. S., Potrich, D. P., Salim, A. C., Santos, F. R., Schmitt, R., Schneider, M. P., Schrank, A., Schrank, I. S., Schuck, A. F., Seuanez, H. N., Silva, D. W., Silva, R., Silva, S. C., Soares, C. M., Souza, K. R., Souza,

R. C., Staats, C. C., Steffens, M. B., Teixeira, S. M., Urmenyi, T. P., Vainstein, M. H., Zuccherato, L. W., Simpson, A. J., and Zaha, A. (2005) *J. Bacteriol.* **187,** 5568–5577
26. Courtney, H. S., Hasty, D. L., Li, Y., Chiang, H. C., Thacker, J. L., and Dale, J. B. (1999) *Mol. Microbiol.* **32,** 89–98
27. Jung, C. J., Zheng, Q. H., Shieh, Y. H., Lin, C. S., and Chia, J. S. (2009) *Mol. Microbiol.* **74,** 888–902
28. Fischetti, V. A., Jones, K. F., and Scott, J. R. (1985) *J. Exp. Med.* **161,** 1384–1401
29. Kelly, C., Evans, P., Bergmeier, L., Lee, S. F., Progulske-Fox, A., Harris, A. C., Aitken, A., Bleiweis, A. S., and Lehner, T. (1989) *FEBS Lett.* **258,** 127–132
30. Scarman, A. L., Chin, J. C., Eamens, G. J., Delaney, S. F., and Djordjevic, S. P. (1997) *Microbiology* **143,** 663–673
31. Bordier, C. (1981) *J. Biol. Chem.* **256,** 1604–1607
32. Scott, N. E., Marzook, N. B., Deutscher, A., Falconer, L., Crossett, B., Djordjevic, S. P., and Cordwell, S. J. (2010) *Proteomics* **10,** 277–288
33. Cordwell, S. J., Len, A. C., Touma, R. G., Scott, N. E., Falconer, L., Jones, D., Connolly, A., Crossett, B., and Djordjevic, S. P. (2008) *Proteomics* **8,** 122–139
34. Zhang, K., McKinlay, C., Hocart, C. H., and Djordjevic, M. A. (2006) *J. Proteome Res.* **5,** 3355–3367
35. Szczepanek, S. M., Frasca, S., Jr., Schumacher, V. L., Liao, X., Padula, M., Djordjevic, S. P., and Geary, S. J. (2010) *Infect. Immun.* **78,** 3475–3483
36. Nunomura, K., Nagano, K., Itagaki, C., Taoka, M., Okamura, N., Yamauchi, Y., Sugano, S., Takahashi, N., Izumi, T., and Isobe, T. (2005) *Mol. Cell. Proteomics* **4,** 1968–1976
37. Altschul, S. F., Madden, T. L., Schäffer, A. A., Zhang, J., Zhang, Z., Miller, W., and Lipman, D. J. (1997) *Nucleic Acids Res.* **25,** 3389–3402
38. Altschul, S. F., Wootton, J. C., Gertz, E. M., Agarwala, R., Morgulis, A., Schäffer, A. A., and Yu, Y. K. (2005) *FEBS J.* **272,** 5101–5109
39. Gasteiger, E., Hoogland, C., Gattiker, A., Duvaud, S., Wilkins, M. R., Appel, R. D., and Bairoch, A. (2005) in *The Proteomics Protocols Handbook* (Walker, J. M., ed) pp. 571–607, Humana Press Inc., Totowa, NJ
40. Lupas, A., Van Dyke, M., and Stock, J. (1991) *Science* **252,** 1162–1164
41. McDonnell, A. V., Jiang, T., Keating, A. E., and Berger, B. (2006) *Bioinformatics* **22,** 356–358
42. Wolf, E., Kim, P. S., and Berger, B. (1997) *Protein Sci.* **6,** 1179–1189
43. Bendtsen, J. D., Nielsen, H., von Heijne, G., and Brunak, S. (2004) *J. Mol. Biol.* **340,** 783–795
44. Nielsen, H., Engelbrecht, J., Brunak, S., and von Heijne, G. (1997) *Protein Eng.* **10,** 1–6
45. Sonnhammer, E. L., von Heijne, G., and Krogh, A. (1998) *Proc. Int. Conf. Intell. Syst. Mol. Biol.* **6,** 175–182
46. Peng, K., Radivojac, P., Vucetic, S., Dunker, A. K., and Obradovic, Z. (2006) *BMC Bioinformatics* **7,** 208
47. Obradovic, Z., Peng, K., Vucetic, S., Radivojac, P., and Dunker, A. K. (2005) *Proteins* **61,** Suppl. 7, 176–182
48. Jenkins, C., Wilton, J. L., Minion, F. C., Falconer, L., Walker, M. J., and Djordjevic, S. P. (2006) *Infect. Immun.* **74,** 481–487
49. Scott, N. E., Bogema, D. R., Connolly, A. M., Falconer, L., Djordjevic, S. P., and Cordwell, S. J. (2009) *J. Proteome Res.* **8,** 4654–4664
50. Hellström, J. L., Vehniäinen, M., Mustonen, M., Lövgren, T., Lamminmäki, U., and Hellman, J. (2006) *Biochim. Biophys. Acta* **1764,** 1735–1740
51. Proft, T., Hilbert, H., Plagens, H., and Herrmann, R. (1996) *Gene* **171,** 79–82
52. Belloy, L., Vilei, E. M., Giacometti, M., and Frey, J. (2003) *Microbiology* **149,** 185–193
53. Zimmermann, L., Peterhans, E., and Frey, J. (2010) *J. Bacteriol.* **192,** 3773–3779
54. de Castro, L. A., Rodrigues Pedroso, T., Kuchiishi, S. S., Ramenzoni, M., Kich, J. D., Zaha, A., Henning Vainstein, M., and Bunselmeyer Ferreira, H. (2006) *Vet. Microbiol.* **116,** 258–269
55. Uversky, V. N., and Dunker, A. K. (2010) *Biochim. Biophys. Acta* **1804,** 1231–1264
56. Coutte, L., Alonso, S., Reveneau, N., Willery, E., Quatannens, B., Locht, C., and Jacob-Dubuisson, F. (2003) *J. Exp. Med.* **197,** 735–742
57. Wright, H. T. (1991) *Protein Eng.* **4,** 283–294
58. Dunker, A. K., and Obradovic, Z. (2001) *Nat. Biotechnol.* **19,** 805–806
59. Hsu, T., Artiushin, S., and Minion, F. C. (1997) *J. Bacteriol.* **179,** 1317–1323
60. Linden, S. K., Sutton, P., Karlsson, N. G., Korolik, V., and McGuckin, M. A. (2008) *Mucosal. Immunol.* **1,** 183–197
61. Menozzi, F. D., Pethe, K., Bifani, P., Soncin, F., Brennan, M. J., and Locht, C. (2002) *Mol. Microbiol.* **43,** 1379–1386
62. Moelleken, K., and Hegemann, J. H. (2008) *Mol. Microbiol.* **67,** 403–419
63. Agarwal, V., Asmat, T. M., Luo, S., Jensch, I., Zipfel, P. F., and Hammerschmidt, S. (2010) *J. Biol. Chem.* **285,** 23486–23495
64. Baron, M. J., Filman, D. J., Prophete, G. A., Hogle, J. M., and Madoff, L. C. (2007) *J. Biol. Chem.* **282,** 10526–10536
65. Rabenstein, D. L. (2002) *Natural Product Reports* **19,** 312–331
66. Sobel, M., Soler, D. F., Kermode, J. C., and Harris, R. B. (1992) *J. Biol. Chem.* **267,** 8857–8862
67. Hsu, T., and Minion, F. C. (1998) *Infect. Immun.* **66,** 4762–4766
68. Gonciarz-Swiatek, M., and Rechsteiner, M. (2006) *Mol. Immunol.* **43,** 1993–2001
69. Realini, C., and Rechsteiner, M. (1995) *J. Biol. Chem.* **270,** 29664–29667
70. Realini, C., Rogers, S. W., and Rechsteiner, M. (1994) *FEBS Lett.* **348,** 109–113
71. Boesen, T., Fedosova, N. U., Kjeldgaard, M., Birkelund, S., and Christiansen, G. (2001) *Protein Sci.* **10,** 2577–2586